PERK (EIF2AK3) Regulates Proinsulin Trafficking and Quality Control in the Secretory Pathway

Sounak Gupta, Barbara McGrath, and Douglas R. Cavener

OBJECTIVE—Loss-of-function mutations in *Perk* (EIF2AK3) result in permanent neonatal diabetes in humans (Wolcott-Rallison Syndrome) and mice. Previously, we found that diabetes associated with *Perk* deficiency resulted from insufficient proliferation of β-cells and from defects in insulin secretion. A substantial fraction of PERK-deficient β-cells display a highly abnormal cellular phenotype characterized by grossly distended endoplasmic reticulum (ER) and retention of proinsulin. We investigated over synthesis, lack of ER-associated degradation (ERAD), and defects in ER to Golgi trafficking as possible causes.

RESEARCH DESIGN AND METHODS—ER functions of PERK were investigated in cell culture and mice in which *Perk* was impaired or gene dosage modulated. The $Ins2^{+/Akita}$ mutant mice were used as a model system to test the role of PERK in ERAD.

RESULTS—We report that loss of *Perk* function does not lead to uncontrolled protein synthesis but impaired ER-to-Golgi anterograde trafficking, retrotranslocation from the ER to the cytoplasm, and proteasomal degradation. PERK was also shown to be required to maintain the integrity of the ER and Golgi and processing of ATF6. Moreover, decreasing *Perk* dosage surprisingly ameliorates the progression of the *Akita* mutants toward diabetes.

CONCLUSIONS—PERK is a positive regulator of ERAD and proteasomal activity. Reducing PERK activity ameliorates the progression of diabetes in the Akita mouse, whereas increasing PERK dosage hastens its progression. We speculate that PERK acts as a metabolic sensor in the insulin-secreting β-cells to modulate the trafficking and quality control of proinsulin in the ER relative to the physiological demands for circulating insulin.
***Diabetes* 59:1937–1947, 2010**

Dysfunctions in insulin synthesis and secretion causes or contributes to all forms of diabetes, and understanding the underlying molecular pathology of these dysfunctions has been a dominant focus in diabetes research. Studies on the regulation of insulin synthesis and secretion have largely focused on the initial stages of synthesis and the mechanisms of stimulated insulin secretion, but much less is known about the intervening regulation of proinsulin maturation and trafficking that occurs in the secretory pathway organelles including the endoplasmic reticulum (ER) and Golgi complex (1–4). Proinsulin is cotranslationally translocated into the lumen of the ER, where it is initially folded and intramolecular disulfide bonds are formed (4,5). Proinsulin must pass a rigorous quality-control system in the ER before advancing to the Golgi and secretory granules, where the C-peptide is removed and mature insulin is packaged into secretory vesicles.

A deficiency of PERK in humans is the cause of the Wolcott-Rallison Syndrome (WRS), which includes permanent neonatal diabetes (6). Loss-of-function mutations of the mouse *Perk* gene result in the same syndrome of traits seen in human WRS, including permanent neonatal diabetes, exocrine pancreas atrophy, osteopenia, growth retardation, and recurrent hepatitis (7–12). Initial studies showed that diabetes was caused by insulin insufficiency associated with low β-cell mass at the time overt diabetes appeared during neonatal development. By using tissue-specific *Perk* knockout and rescue strains, we established that expression of the *Perk* gene in the β-cells is required for the normal proliferation responsible for the rapid accretion of β-cell mass during embryonic and neonatal development and is required for normal insulin synthesis and secretion. Critically, we found that expression of *Perk* only in the β-cells rescues the diabetes and β-cell defects (7,11). These studies also found that the initial claims (8,9) that low β-cell mass was caused by dysfunctions in the ER stress response and β-cell death were incorrect (11); however, the cause of the multiple defects seen within β-cells was not established. Among the defects observed in *Perk*-deficient β-cells, the most apparent is a massive accumulation and retention of proinsulin in the ER that is first seen during fetal development immediately after endocrine progenitor cells begin to differentiate into insulin-expressing β-cells (11). The aberrant accumulation of proinsulin in the ER could be caused by a number of possible defects including dysfunctions in quality control, proinsulin trafficking, or uncontrolled protein synthesis.

RESEARCH DESIGN AND METHODS

Antibodies. The following antibodies were used: golgin 97 (Abcam), GM130 (BD Biosciences), FK2 (Biomol), HA (Cell Signaling), V5 (Invitrogen), insulin (Linco), proinsulin (Beta Cell Biology Consortium and Hytest), proinsulin C-peptide (Millipore), c-*myc* 9E10, glucagon (Santa Cruz), ERGIC-53 (p58), green fluorescent protein, α-tubulin (Sigma), calnexin, and Erp72 (Stressgen). The CT-A antibody was a gift from the Lencer Lab, and the C8 proteasome subunit antibody (AbC8) was a gift from the Monaco Lab. The in situ cell death detection kit, TMR Red (Roche), was used to detect transferase-mediated dUTP nick-end labeling (TUNEL) cells.

Cell culture, cloning, and transfections. Vesicular stomatitis virus G-protein (*ts045*-VSVG-GFP) in pcDNA3.1 was provided by Jennifer Lippincott-Schwartz (41). Human wild-type proinsulin and the human C(B19)A proinsulin mutant in pcDNA3.1 were from Peter Arvan (42). The pCMV*short*-EYFP-ATF6α in pEYFO-C1 was provided by Kazutoshi Mori (43), pCGN-HA-S2P was obtained from Ron Prywes (18), and C terminus deleted 9E10-tagged mouse PERK (*DNPerk*) in pcDNA was provided by David Ron (44). Transduction of cells with *DNPerk* reduces phosphorylation of eIF2α to 26% normal (13) similar to the reduction seen in *Perk KO* pancreata (9). Wild-type and mutant

From the Department of Biology, The Huck Institutes of the Life Sciences, Penn State Institute for Diabetes and Obesity, Pennsylvania State University, University Park, Pennsylvania.
Corresponding author: Douglas R. Cavener, drc9@psu.edu.
Received 20 July 2009 and accepted 14 May 2010. Published ahead of print at http://diabetes.diabetesjournals.org on 8 June 2010. DOI: 10.2337/db09-1064.

proinsulin genes were subcloned into pIRESbleo3 with a V5 epitope at the C terminus. The wild-type proinsulin-KDEL construct was generated by inserting a KDEL ER-retention sequence 3′ to the V5 epitope-tag. A small-interfering RNA (siRNA) directed against human *Perk* mRNA coding region nucleotides 2,237–2,255 was used to knockdown PERK (45) in human-derived cells lines. Standard transfection protocols were followed (31,45). AD293 and HepG2 cells were cultured in high-glucose DMEM and 10% FBS at 37°C in 5% CO_2. A short-hairpin RNA directed against the rat *Perk* mRNA (*shPerk*) and scramble, randomized sequence (*shScram*) were from Fumihiko Urano (Program in Gene Function and Expression, University of Massachusetts). The *shPerk* and *shScram* are stably integrated into the genome of INS1 832/13 β-cell lines and under the inducible regulation of doxycycline.

Proinsulin and protein synthesis. Proinsulin synthesis was determined as previously described (8). For protein synthesis islets or cultured cells were labeled with S^{35} labeled Met/Cys (500 μCi/ml) at 37°C for 30 min, precipitated with 10% trichloroacetic acid. Radioactivity was measured by scintillation counting and normalized to protein content.

20S proteasomal and retrotranslocation assays. Chymotryptic activity of the proteasome in cell lysates was determined using the 20S Proteasome Activity Assay Kit (Chemicon) (46). The cleavage of LLVY-AMC and release of fluorigenic AMC was measured (360/460 nm) to determine relative proteasome activity. Retrotranslocation assays were performed as previously described (21). Cholera toxin (CT) A (CTA) and CTA1 CT subunits were detected by Western blot.

Trafficking assays. For trafficking assays *ts045* VSVG-GFP was transfected into cells. At 8 h posttransfection, cells were transferred to the restrictive temperature of 40°C for 16 h followed by a shift to the permissive temperature of 32°C for 15 min (unless otherwise specified). Cells were then harvested for immunofluorescence, subcellular fractionation, and EndoH assays (47). The VSVG protein was detected using an antibody to the GFP-tag.

Genetic strains. The *Perk KO* mice strains (9) were congenic for C57BL/6J or 129SvEvTac or were of mixed background, and each strain exhibited the defects described herein. To increase the *Perk* dosage in the β-cells of *Perk KO* mice, a *Perk* transgene under the control of the rat insulin promoter (*βPerk*) was introduced (7). Mice bearing the *Akita* mutation in a C57BL/6J background were from The Jackson Laboratories. These mice were crossed into $Perk^{+/-}$, *βPerk* mice to generate the strains used. The *Akita* mutants (C57BL/6J) were crossed with $Perk^{+/-}$ in the 129SvEvTac background to generate $Ins2^{+/Akita}$, $Perk^{+/-}$ double heterozygotes or $Ins2^{+/Akita}$, $Perk^{+/+}$ mice that were F1 hybrids. All other strains were in a mixed genetic background. All animal studies were approved by the institutional animal care and use committee of Pennsylvania State University.

Islet isolation. Islets were isolated using a modified histopaque-1077 separation method (11). Islets were cultured in RPMI for 6–12 h at 37°C in 5% CO_2 prior to experimental processing.

In vivo glucose-stimulated insulin secretion and total pancreatic insulin content. For studies of in vivo glucose-stimulated insulin secretion (GSIS), serum was collected after a 16-h fast and 20 min after the intraperitoneal injection of 2 mg glucose/g body wt. Serum insulin concentrations were determined by immunoassay (Meso Scale Discovery). For total pancreatic insulin measurement, pancreata were sonicated in 1 ml of acid ethanol (95% ethanol:10.2N HCl in a 50:1 ratio), incubated overnight at 4°C, centrifuged and the supernatant assayed for insulin.

Statistical analysis. Statistical analysis was performed using Student *t* test, and $P < 0.05$ was accepted as significant. Error bars represent the SE of the mean.

RESULTS

PERK-deficient mice exhibit abnormal β-cell morphology but normal steady-state protein synthesis rates. In wild-type β-cells (Fig. 1*A* and *B*), proinsulin was found to be localized in a perinuclear pattern within the Golgi (Fig. 1*C*), as previously reported (5). A substantial fraction (ca 30–40%) of PERK-deficient β-cells exhibit an extremely distorted cellular morphology (Fig. 1*D–F*), which we denote as an impacted-ER phenotype characterized by expanded ER and massive accumulation of proinsulin (Fig. 1*F*, *arrows*) colocalizing with ER markers (11). Quantitative analysis of the signal intensity in wild-type, knockout nonimpacted-, and knockout impacted-ER β-cells revealed that insulin was not significantly different (Fig. 1*G*). Proinsulin levels were not significantly different between wild-type and *Perk KO* nonimpacted-ER β-cells; however, the proinsulin level in the *Perk KO* impacted-ER β-cells is more than sevenfold higher compared with wild-type or *Perk KO* nonimpacted-ER β-cells. Developmental studies by us have suggested that the impacted-ER β-cells in *Perk KO* mice are derived from nonimpacted-ER β-cells (11).

To determine whether uncontrolled synthesis caused overaccumulation of proinsulin in the *Perk KO* impacted-ER β-cell, we examined protein or proinsulin synthesis rates in PERK-deficient cells. We found that global protein synthesis rates in INS1-832/13 (13) and AD293-expressing *DNPerk*, *Perk KO* islets (Fig. 1*H*), and *shPerk*-expressing INS1-832/13 β-cells (Fig. 1*I*) were not significantly different from wild-type controls. In addition, proinsulin synthesis is actually somewhat reduced in *shPerk* INS1-832/13 β-cells (Fig. 1*I*). Therefore, the abnormal accumulation of proinsulin in the ER is not caused by uncontrolled or derepressed proinsulin synthesis and is not correlated with an increase in general protein synthesis. Moreover, insulin and proinsulin content in the *Perk KO* nonimpacted β-cells are not elevated (Fig. 1*G*) as would be expected if proinsulin synthesis was derepressed.

Suppression of PERK activity leads to an ER-Golgi anterograde trafficking defect. Abnormal accumulation of proinsulin in the ER of PERK-deficient β-cells could be caused by defects in ER-Golgi trafficking, and to address this question we assessed the trafficking of the temperature-sensitive variant of the *ts045* VSVG-GFP (14) in cells in which PERK activity was suppressed by a dominant-negative mutation of *Perk* (*DNPerk*). We found that suppressing PERK activity in HepG2 (Fig. 2*A–D*), INS-1 832/13 (Fig. 2*E–H*) and AD293 (Fig. 2*I–R*, supplementary Fig. S1*E*, available at http://diabetes.diabetesjournals.org/cgi/content/full/db09-1064/DC1) cells blocked anterograde movement of *ts045* VSVG-GFP from the ER to the Golgi compared with vector-transfected control cells (supplementary Fig. S1*A–D*). This trafficking defect was also confirmed using the EndoH-resistance assay in AD293 cells (Fig. 2*S*), which showed an almost complete block in anterograde trafficking of VSVG following a shift to the permissive temperature.

Suppression of PERK activity results in redistribution of Golgi components into the ER. To examine whether Golgi components were redistributed into the ER in PERK-suppressed cells as a consequence of the trafficking defect, we carried out subcellular fractionation (SCF) analysis. For this purpose, AD293 cells cotransfected with *ts045* VSVG-GFP and *DNPerk* were incubated overnight at the restrictive temperature followed by a shift to the permissive temperature for 15 min. Equivalent numbers of cells were then harvested for SCF. In the empty-vector controls, VSVG was successfully trafficked from the ER-enriched fractions (fractions 7–9) to the ER-Golgi intermediate compartment (ERGIC) and partially into the Golgi (Fig. 3*A*). In contrast, in the *DNPerk* cotransfected cells the VSVG cargo was retained within the ER-enriched fractions (fractions 7–9) (Fig. 3*B*). In these cells, the marker for the ERGIC compartment was redistributed into the ER-enriched fractions, while the Golgi marker, golgin, showed very low levels of expression relative to the ER marker calnexin (Fig. 3*B*).

Immunohistochemical (IHC) analysis revealed an impacted-ER phenotype due to abnormal ER retention of misfolded *ts045* VSVG-GFP in AD293 cells, in which PERK activity was suppressed by *DNPerk* (supplementary Fig. S1*E*, *arrowheads*) (Fig. 2*C*, *G*, and *K*) or by *Perk* siRNA–mediated knockdown (Fig. 2*M* and *P*). In addition, the

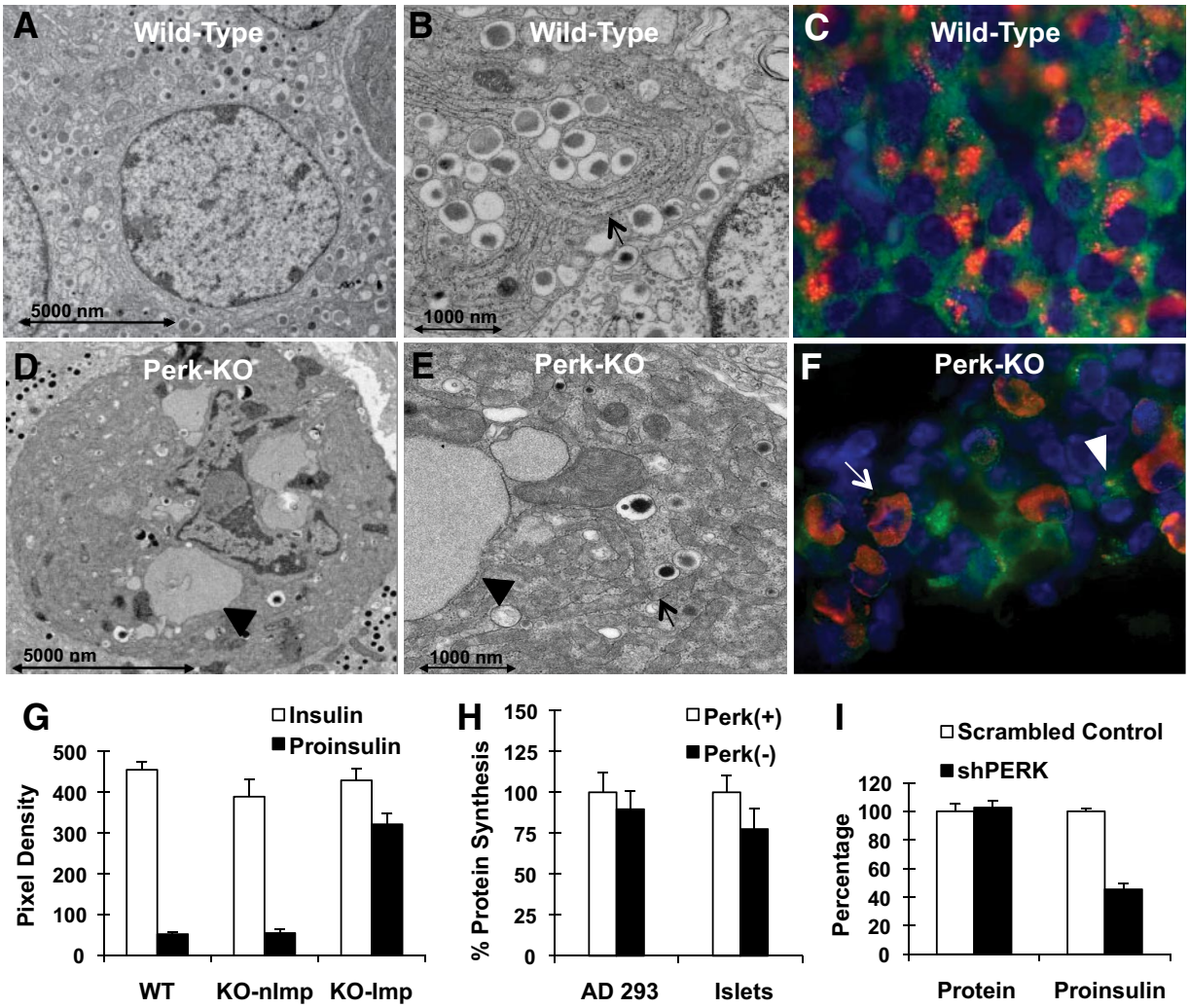

FIG. 1. PERK-deficient mice exhibit an abnormal β-cell morphology (*A–F*) and normal steady-state protein synthesis (*G*). *A*: TEM image of a normal β-cell from a P1 wild-type mouse. *B*: At higher magnification, the normal laminar morphology of the ER and associated ribosomes can be seen in the wild-type β-cell (*arrow*). *C*: IHC image of a normal β-cell from a P1 wild-type mouse showing proinsulin (red) within the Golgi and insulin (green) throughout the cytoplasm. Nuclei are stained with DAPI (blue). Pancreata were isolated, fixed, and prepared for IHC analysis as previously described (9). *D*: TEM image of a *Perk KO* β-cell from a P1 mouse. *E*: At higher magnification, the overall abnormal ER morphology (*arrow*) and frequent ribosome-studded balloon-like structures (*arrow head*) can be readily detected. *F*: IHC staining for proinsulin in *Perk KO* β-cells from a P1 mouse shows a subpopulation of cells with abnormal distribution of proinsulin throughout the cytoplasm that colocalizes with ER markers (11). *G*: Quantitative analysis of insulin and proinsulin levels were performed on IHC images of β-cells in postnatal day 1 *Perk KO* and wild-type littermates. All procedures and reagents for histochemical preparation and image collection were done at the same time under identical conditions to allow direct comparison of signal density area estimates of insulin and proinsulin between genotypes and individuals. Area density analysis was performed using NIH Image J on clusters of β-cells within islets or on individual β-cells so as to exclude other endocrine cell types. Background subtraction was performed by subtracting nonspecific pixel density calculated from the adjacent exocrine pancreas. A total of 16–18 islets were analyzed for two individual littermates per genotype. To compare impacted-ER β-cells with nonimpacted-ER β-cells in *Perk KO* mice, 40 individual β-cells each were analyzed. Average pixel densities, after background subtraction, are shown without any form of normalization. KO Imp, *Perk KO*, impacted-ER phenotype; KO nImp, *Perk KO*, nonImpacted-ER phenotype. *H*: Cells were cultured in 11 mmol/l glucose prior to the addition of S^{35}-labeled cysteine and methionine. For AD293 cells *Perk* (+) represents empty vector and *Perk* (−) represents cells impaired for *Perk* activity by *DNPerk*. For islets *Perk* (+) represents wild-type neonatal islets (n = 16) and *Perk* (−) (n = 8) represents islets isolated from neonatal *Perk KO* mice. Differences are not statistically significant ($P > 0.05$). *I*: Global and proinsulin synthesis was assessed in INS1 832/13 cells in which *Perk* was ablated by expression of *shPerk* as compared with a scramble control (*shScram*). The level of rat *Perk* mRNA and protein were reduced by 60–70% and 56–66%, respectively, at 48 h after the induction of the expression of shRNAs by treatment with 2 mg/ml doxycycline in INS1-832/13 β-cells. Cells were pulse-labeled with S^{35}-labeled cysteine and methionine for 30 min, and cellular extracts were either TCA precipitated for analysis of global protein synthesis or immunoprecipitated with proinsulin antibody followed by electrophoretic separation. (A high-quality digital representation of this figure is available in the online issue.)

Golgi marker GM130 appeared to be dispersed throughout the cytoplasm (Fig. 2*B*, *F*, *J*, *N*, and *Q*). Similarly, in *Perk KO* impacted-ER β-cells, GM130 was no longer condensed into perinuclear structures but instead was redistributed throughout the cytoplasm (Fig. 3*C–E*). The localization of the ERGIC marker protein ERGIC-53 was examined to determine whether defects in the intermediate compartment were also present in *Perk KO* impacted-ER β-cells. We found that in wild-type β-cells the ERGIC compartment forms a previously unidentified structure that encircles a large concentration of proinsulin in wild-type β-cells (Fig. 3*F–H*). However, in *Perk*-deficient impacted-ER β-cells, the ERGIC compartment was dispersed and was no longer in juxtaposition to proinsulin (Fig. 3*I–K*, *box*). In addition, the level of proinsulin was reduced in the ERGIC compartment in the nonimpacted-ER β-cells (Fig. 3*I–K*, *arrows*).

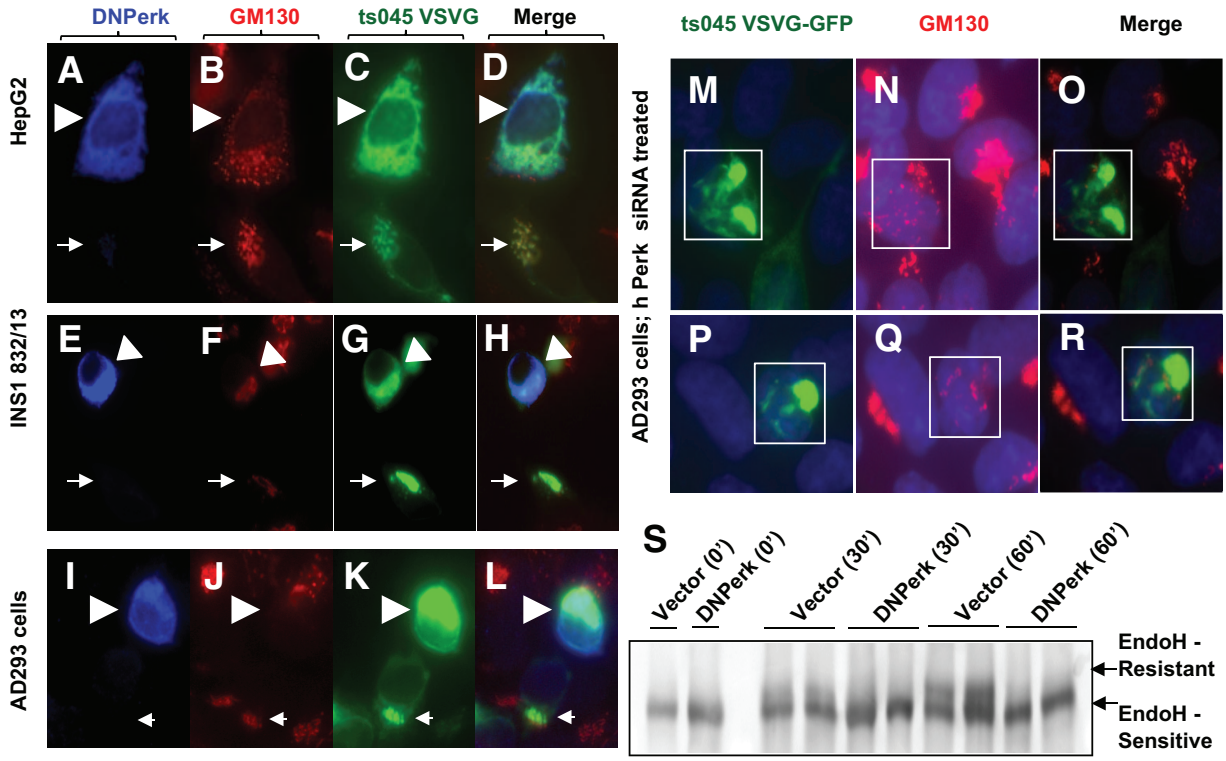

FIG. 2. An acute ablation of *Perk* function leads to an ER to Golgi anterograde trafficking defect. IHC in HepG2 cells (*A–D*), INS1 (832/13) (*E–H*), AD293 cells (*I–R*), and EndoH resistance assay in AD293 cells (*S*). *A–L*: Cells were cultured on Lab-Tec (Nalge Nunc) chamber slides prior to transfection with *DNPerk* and *ts045* VSVG-GFP followed by IHC analysis of detergent-permeabilized cells (0.2% Triton X 100 in 1 × PBS for 10 min at room temperature). *Arrowheads* show a *DNPerk* and *ts045*-VSVG-GFP cotransfected cell following a 16-h incubation at the restrictive temperature and a 15-min shift to the permissive temperature. *Arrows* indicate an adjacent control cell transfected with only *ts045*-VSVG-GFP. *A–D*: HepG2 cells were cotransfected with c-*myc* tagged *DNPerk* (blue, *A*) and *ts045*-VSVG-GFP (green, *C*) and stained for the Golgi marker GM130 (red, *B*). The merged image is seen in *D*. *E–H*: INS1 (832/13) cells were cotransfected with c-*myc*–tagged *DNPerk* (blue, *E*) and *ts045*-VSVG-GFP (green, *G*) and stained for the Golgi marker GM130 (red, *F*). The merged image is seen in *H*. *I–L*: AD293 cells were cotransfected with c-*myc*–tagged *DNPerk* (blue, *I*) and *ts045*-VSVG-GFP (green, *K*) and stained for the Golgi marker GM130 (red, *J*). The merged image is seen in *L*. *M–R*: IHC in AD293 cells. *Boxed areas* in *M* and *P* show cells cotransfected with *ts045* VSVG-GFP (green) and *Perk* siRNA after an 8-h incubation at the restrictive temperature followed by a 15-min shift to the permissive temperature. Human *Perk* mRNA was reduced by 41% at 8 h posttransfection of the siRNA. Staining for the Golgi marker GM130 shows a dispersed morphology in red (*N* and *Q*) and the merged images are seen in *O* and *R*. *S*: *ts045*-VSVG-GFP was cotransfected with either empty vector (Vector) or *DNPerk* into AD293 cells. Cells were incubated overnight at the restrictive temperature to allow the VSVG to accumulate in the ER (0′). Cells were then shifted to the permissive temperature to allow the protein to traffic to the Golgi. Cells were harvested for EndoH treatment and Western blots at the indicated time points. The higher MW form (*upper arrow*) is the EndoH-resistant Golgi form, while the *lower arrow* indicates the ER-retained EndoH-sensitive form. (A high-quality digital representation of this figure is available in the online issue.)

ATF6 processing is constitutively activated in *Perk*-deficient cells. ATF6 positively regulates ERp72 and GRP78/BiP (15) and also represses insulin gene transcription (16) and therefore may be the cause of induction these two ER chaperones (13) in PERK-deficient β-cells as well as the reduced insulin gene expression that we reported previously (11). ATF6 is an ER resident protein that upon induction is trafficked to the Golgi where it is processed by the site 1 and 2 proteases (S1P and S2P, respectively) to generate the mature transcriptionally active form of ATF6 (17). We observed a constitutive reduction in full-length ATF6 and induction of the cleaved nuclear form (Fig. 4). In addition, S2P was found to be abnormally redistributed into the ER of PERK-suppressed cells (supplementary Fig. S2). These findings are consistent with previous reports that redistribution of Golgi proteases to the ER caused by a pharmacological block in trafficking can result in constitutive processing of ATF6 (18). Associated with the redistribution of Golgi components, we found substantial changes in the lipid composition of the ER and Golgi (supplementary Fig. S3*A* and *B*). Because overexpression of DNPERK protein may effect lipid composition and other associated defects in the ER for reasons other than suppressing PERK activity, these results need to be confirmed by ablating *Perk* via siRNA methods.

ERAD is impaired in PERK-suppressed cells. A large fraction of all newly synthesized cargo proteins in the ER fail to attain their native conformation (19), and these proteins undergo ERAD, which is comprised of three steps: ER-cytosolic retrotranslocation, ubiquitylation, and, finally, proteasome-mediated degradation (20). Retrotranslocation from the ER to the cytoplasm was examined by monitoring the fate of CT subunits targeted to the ER (21) (Fig. 5*A*). Suppression of PERK in AD293 cells substantially reduced the amount of retrotranslocated CTA1 CT subunit, suggesting that *Perk* is necessary for retrotranslocation activity. ERp72, a protein disulfide isomerase-like chaperone, is localized in the ER and is a negative regulator of retrotranslocation (21). Suppression of PERK activity in AD293 cells led to a 3.3-fold induction in ERp72 protein levels (Fig. 5*B*), and this was correlated with the localization of ERp72 to large balloon-like structures in impacted-ER β-cells (Fig. 1*D* and *E*, *arrowheads*) seen in *Perk KO* mice (13).

To examine the fate of proinsulin in the ER, independent of anterograde trafficking, we expressed proinsulin containing an ER retention signal (Ins^{+}-KDEL) (supple-

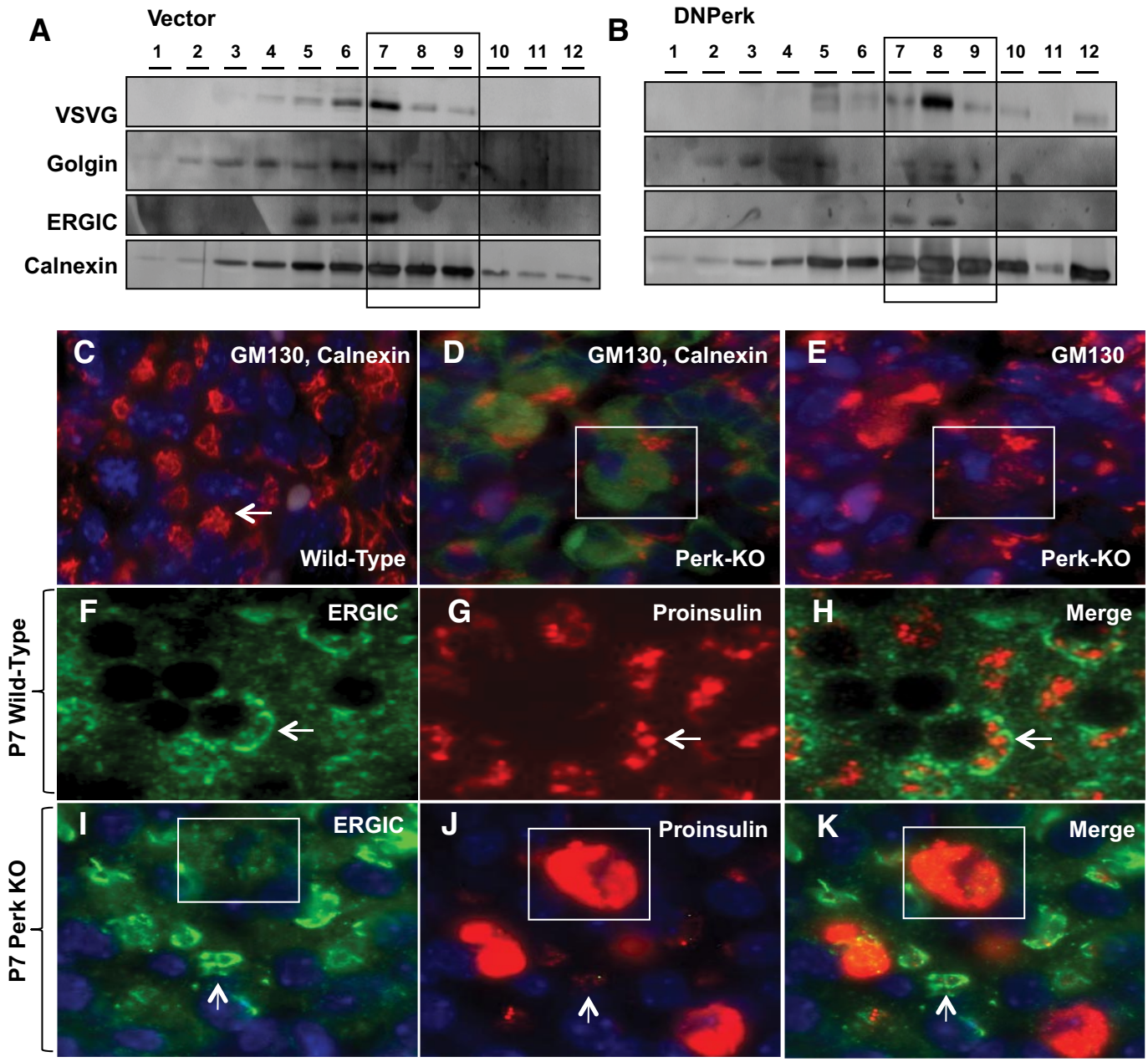

FIG. 3. Impaired ER-Golgi anterograde trafficking leads to a redistribution of the Golgi compartment into the ER. *A* and *B*: Representative data from two independent experiments involving subcellular fractionation in PERK-suppressed AD293 cells. IHC in P7 wild-type islets (*C* and *F–H*) and P7 *Perk KO* islets (*D*, *E* and *I–K*). *A* and *B*: AD293 cells were cotransfected with either an empty vector (Vector) and *ts045* VSVG-GFP (*A*) or *DNPerk* and *ts045* VSVG-GFP (*B*). Equivalent amounts of protein were subjected to subcellular fractionation following a 16-h incubation at the restrictive temperature and a 15-min shift to the permissive temperature. Cells were harvested into 0.25 mol/l sucrose, 1 mmol/l EDTA, 10 mmol/l Tris HCl (pH 7.4), supplemented with protease inhibitors. Homogenization was carried out in a ball-bearing homogenizer followed by centrifugation at 800*g* for 10 min at 4°C. Equivalent amounts of supernatant protein were loaded on 4–35% Optiprep gradients and centrifuged in a SW41Ti rotor at 125,000*g* for 1 h and 45 min at 4°C in a Beckman l8-80M ultracentrifuge. Twelve equal fractions were collected and prepared for Western blotting by TCA precipitation. The first fraction represents the top of the gradient and the twelfth fraction represents the pellet. *A* and *B*: Immunoblotting for calnexin (ER marker, *bottom panel*), ERGIC-53 (intermediate compartment marker, *third panel*), golgin (Golgi marker, *second panel*), and the trafficked cargo VSVG (*top panel*). *Boxed areas* show ER-enriched fractions (7–9). *C* and *D*: Staining for GM130 (red), calnexin (green), and nuclear staining with DAPI (blue) is shown in islets from wild-type (*C*) and P1 *Perk KO* littermates (*D*) stained for calnexin and GM130. *Arrow* shows Golgi morphology in a normal β-cell (*C*) with low basal levels of calnexin expression (not apparent at this exposure but seen in longer exposure in cytoplasm). GM130 and DAPI are stained for in *Perk* KO mice in *E*. The boxed area (*D* and *E*) shows a representative impacted-ER β-cell demonstrating increased calnexin expression (*D*) and diffuse GM130 staining (*D* and *E*). *F–K*: Staining for ERGIC-53 (*F* and *I*), proinsulin (*G* and *J*), and the corresponding merged images (*H* and *K*) in islets from wild-type (*F–H*) and P7 *Perk KO* (*I–K*) islets. *Arrows* (*I-K*) show quasinormal ER β-cells and the *boxed areas* show a representative impacted-ER β-cell. Quasinormal-ER β-cells (*arrow*, 3*J*) have dramatically reduced proinsulin signal. (A high-quality digital representation of this figure is available in the online issue.)

mentary Fig. S4*A* and *B*). Following cotransfection of Ins^{+}-KDEL with *DNPerk* into AD293 cells, we noted multiple high–molecular weight forms that we identified as ubiquitylated isoforms of proinsulin (Fig. 5*C*). We also found a highly significant 3.6-fold increase in the accumulation of Ins^{+}-KDEL in the PERK-suppressed cells compared with the empty-vector cotransfected controls (Fig. 5*D*), while proinsulin and steady-state protein synthesis levels in these cells showed no significant changes (Fig. 1*H–I*; supplementary Fig. S4*C*). This suggests that the

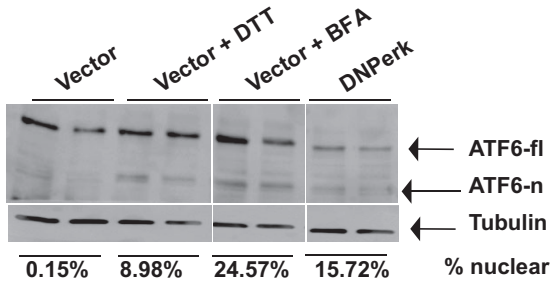

FIG. 4. Basal level of processed ATF6 is elevated in *Perk*-deficient cells. AD293 cells were cotransfected with EYFP-ATF6α and either an empty vector (Vector) or *DNPerk*. Empty-vector cotransfected samples were either left untreated, while samples treated with 5 mmol/l dithiothreitol (DTT) or 5 μg/ml brefeldin A (BFA) for 1 h served as controls for ATF6 induction. Immunoblotting with an antibody that recognizes YFP-tagged ATF6 shows both the ER-resident uncleaved (fl, full length) and cleaved nuclear (n) forms. Quantification of the nuclear ATF6 expressed as a percentage of the full-length form is shown below the tubulin panel.

abnormal accumulation of proinsulin can occur independent of both the anterograde trafficking defect and runaway protein synthesis. PERK-suppressed cells also showed a significant accumulation of the ubiquitylated proinsulin isoforms within the ER (supplementary Fig. S4*D*). This was seen when AD293 cells were cotransfected with *DNPerk* and Ins$^+$-KDEL (55.3% increase) (Fig. 5*D*, *arrow*) or wild-type proinsulin (62% increase) (supplementary Fig. S4*E*, *arrow*), suggesting that they are inefficiently degraded and retained within the ER.

An important step in proteasomal assembly occurs at the ER membrane through the action of proteasome maturation protein (POMP) to form the 20S core complex (22). We found that the amount of the 20S proteasome precursor was greatly diminished in the impacted-ER β-cells of *Perk KO* mice (Fig. 6*A*–*D*), suggesting that assembly or synthesis of the proteasome may be negatively impacted. Additionally, proteasomal activity in islets isolated from neonatal *Perk KO* mice was found to be significantly repressed by 39% (Fig. 6*E*) compared with wild-type littermates, although no reduction in proteasomal activity was found in PERK-suppressed AD293 cells. Moreover, both an acute ablation of *Perk* in INS1 (832/13) β-cells (13), as well as a treatment of these cells with the nonspecific proteasomal inhibitor MG132 (Fig. 6*F* and *G*), phenocopies the accumulation of proinsulin in the ER that is indistinguishable from the impacted-ER β-cells of *Perk KO* mice and *DNPerk*-832/13 cells.

Modulating *Perk* gene dosage alters the progression of *Akita* insulin mutant mice to frank diabetes. The *Akita-Ins2* mutation (C96Y) in mice leads to the develop-

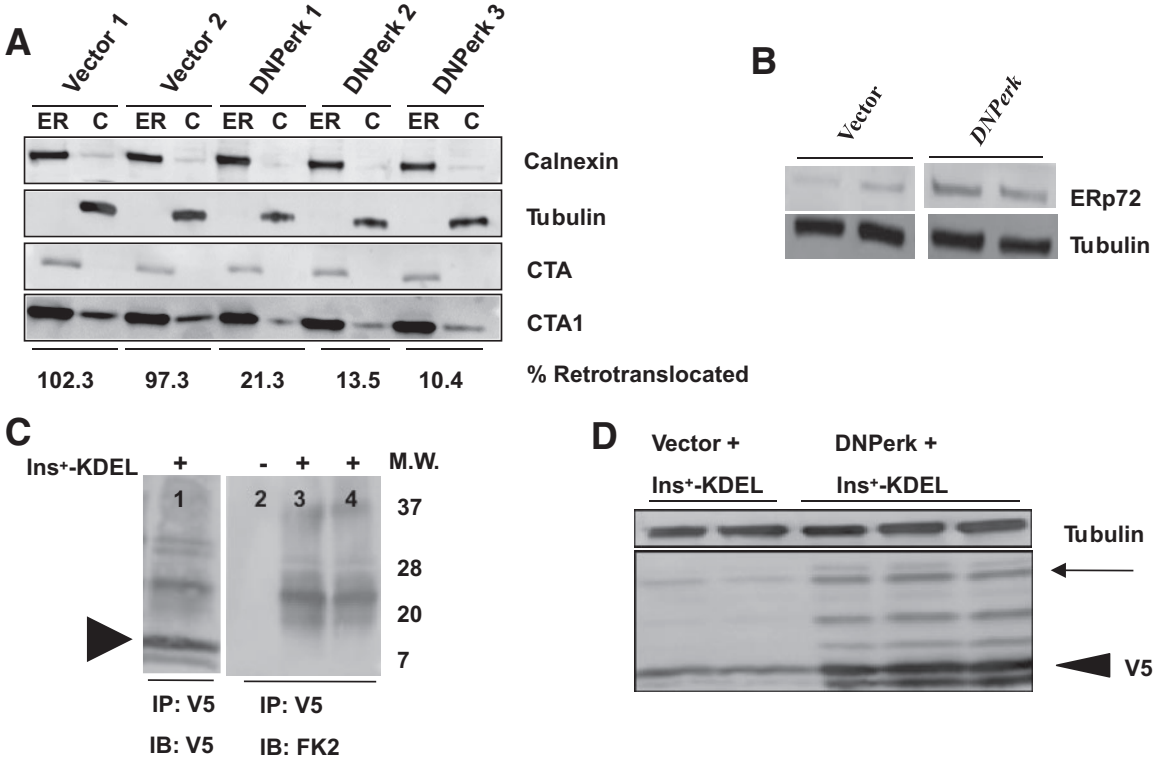

FIG. 5. Impaired ERAD in *Perk*-deficient cells. *A*: Retrotranslocation of CTA1 subunit in PERK-suppressed cells. AD293 cells carrying either empty vector or *DNPerk* were incubated with cholera holotoxin for 90 min. Cells were harvested and separated into cytosolic (C) and ER (ER) fractions and then immunoblotted for calnexin (ER marker), tubulin (cytosolic marker), CTA, or CTA1. Extent of retrotranslocation was quantified by expressing cytosolic CTA1 (normalized to tubulin) as a percentage of ER-retained CTA1 (normalized to calnexin). The percent retrotranslocation in PERK-suppressed cells normalized to empty vector is indicated underneath the immunoblot panels. *B*: Protein extracts from AD293 cells transfected with *DNPerk* or empty vector were immunoblotted for ERp72. Ablation of Perk in AD293 cells resulted in a 3.3-fold increase in ERp72. *C*, *lane 1*: V5-tagged *Ins*$^+$-KDEL was expressed in AD293 cells and was immunoprecipitated and immunoblotted with anti-V5 antibody. *Arrowhead* indicates V5-tagged *Ins*$^+$-KDEL. *Lane 2*: Untransfected control. *Lanes 3* and *4*: *Ins*$^+$-KDEL construct was transfected into AD293 cells and lysates were immunoprecipitated with anti-V5 and then immunoblotted with the FK2 antibody that recognizes mono- and polyubiquitylated species but not free ubiquitin. Molecular weight markers (kd) are shown to the right of the blot. *D*: AD293 cells were cotransfected with V5-tagged wild-type proinsulin-KDEL (*Ins*$^+$-KDEL) and empty vector (Vector) or *DNPerk*. Lysates were immunoblotted with the anti-V5 antibody. *Arrowhead* indicates V5-tagged proinsulin. A 3.6-fold increase in the retention of *Ins*$^+$-KDEL in the PERK-suppressed cells compared with the empty-vector cotransfected controls was noted. The multiple higher–molecular weight bands (*arrow*) are ubiquitylated species as shown in *C*.

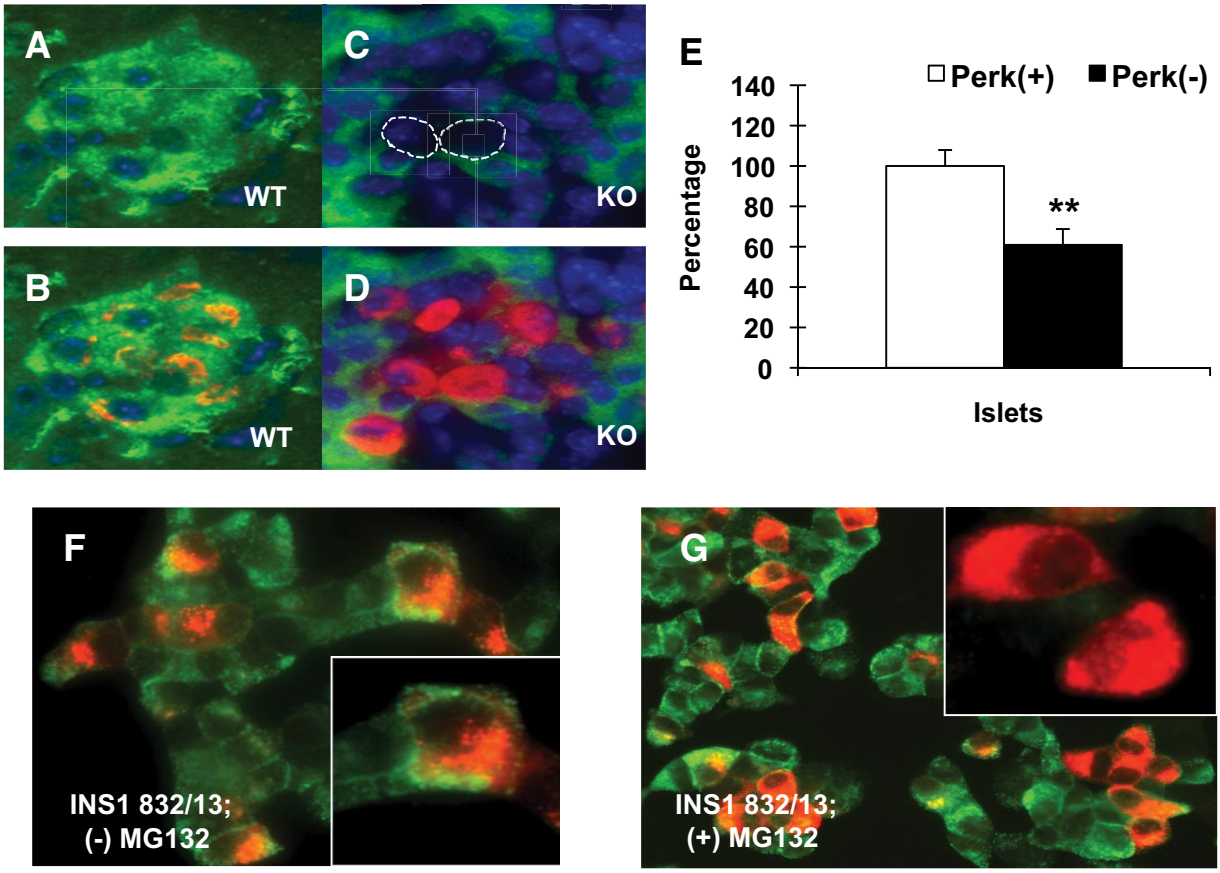

FIG. 6. Impaired proteasome activity in *Perk*-deficient cells. *A*: C8 (PSMA3) proteasome precursor subunit (green) is shown in a P1 wild-type islet. The C8/PSMA3 antibody cross-reacts with proteasome precursor β subunit complexes (48). *B*: Merged image with proinsulin (red) and DAPI (blue). *C*: The amount of C8 is reduced in impacted-ER β-cells (circled) in an islet from a P1 *Perk KO* mouse. *D*: A merged image with proinsulin (red) and DAPI (blue) is shown. *E*: 20S proteasomal activity was measured in islets isolated from neonatal wild-type and *Perk KO* mice (50 islets per sample) by measuring the release of the fluorophore AMC (7-amino-4methylcoumarin) from the synthetic proteasomal substrate peptide LLVY-AMC (20S Proteasomal Assay Kit; Chemicon). AMC fluorescence was measured at 360/340 nm at 1-min intervals over a 1-h period using a FL × 800 Microplate Fluorescence Reader and analyzed using KC Junior software (BioTek Instruments). The above data are a combination of two independent experiments where proteasomal activity in *Perk KO* islets ($n = 9$) was normalized to wild type ($n = 8$) ($P = 0.0034$). *F* and *G*: Insulin staining is shown in green and proinsulin staining is shown in red. *F*: Untreated control 832/13 cells. *Inset* shows normal perinuclear distribution of proinsulin within the Golgi. *G*: 832/13 cells treated with the nonspecific proteasomal inhibitor MG132 (40 μmol/l) for 1 h. *Inset* shows abnormal proinsulin distribution throughout the cytoplasm. (A high-quality digital representation of this figure is available in the online issue.)**

ment of severe hyperglycemia by the postnatal age of 4–6 weeks (23), and the same mutation in the single human insulin gene results in permanent neonatal diabetes (24). Unexpectedly, we found that β-cell mass was expanded in $Ins2^{+/Akita}$ heterozygous mice at the time these mice are rapidly progressing to frank diabetes (Table 1). However,

TABLE 1
Akita insulin mutant mice exhibit β-cell hyperplasia during early progression to diabetes

Genotype	$Ins2^{+/+}$	$Ins2^{+/Akita}$	$Ins2^{+/Akita}$
	$Perk^{+/-}$ and $^{+/+}$	$Perk^{+/-}$ and $^{+/+}$	$\beta Perk^{+}$ $Perk^{+/-}$ and $^{+/+}$
Blood glucose (mg/dl)	136.0	244.1*	297.8†
Average number β-cells per islet	29.6	68.7‡	35.4 (NS)
Percent TUNEL^{+} β-cells	0.37	0.04	0.09
Chop mRNA	100.0 ± 42.7	146.7 ± 48.8 (NS)	150.0 ± 49.4 (NS)

The data shown in this table is representative of mice that belong to the postnatal age group $p14–17$. Serum blood glucose was determined in random fed mice. To estimate β-cell mass and cell death, tissue sections were immunostained for insulin, TUNEL, and DAPI. β-Cells and insulin-positive cells were manually counted for all islets containing more than five β-cells. The average number of β-cells within a cross-section of each islet was calculated. To estimate β-cell death, cells that were insulin and TUNEL positive were manually counted. For IHC analysis, pancreata were harvested from littermates. The number of mice, islets, and β-cells counted were as follows: $Ins2^{+/}$ $Perk^{+/-}$ and $^{+/+}$, mice = 6, islets = 136, and β-cells = 2,172; $Ins2^{+/Akita}$ $Perk^{+/-}$ and $^{+/+}$, mice = 10, islets = 277, and β-cells = 12,777; and $Ins2^{+/Akita}$; $\beta Perk^{+}$ $Perk^{+/-}$ and $^{+/+}$, mice = 6, islets = 136, and β-cells = 3,492. *Chop* mRNA level for each genotype was normalized to $Ins2^{+/+}$; $Perk^{+/-}$ and $P^{+/+}$. For *Chop* mRNA, islets were isolated from littermates ($Ins2^{+/+}$; $Perk^{+/-}$ and $^{+/+}$, $n = 6$; $Ins2^{+/Akita}$; $Perk^{+/-}$ and $^{+/+}$, $n = 2$; $Ins2^{+/Akita}$; $\beta Perk^{+}$ $Perk^{+/-}$ and $^{+/+}$, $n = 4$). Comparison of means (Student t test) showed no significant differences between any of the paired comparisons for Chop mRNA levels. *$P = 0.055$; †$P = 0.0066$; ‡$P = 0.00{,}016$ vs. age-matched controls ($Ins2^{+/+}$; $Perk^{+/-}$ and $^{+/+}$). NS, not significant.

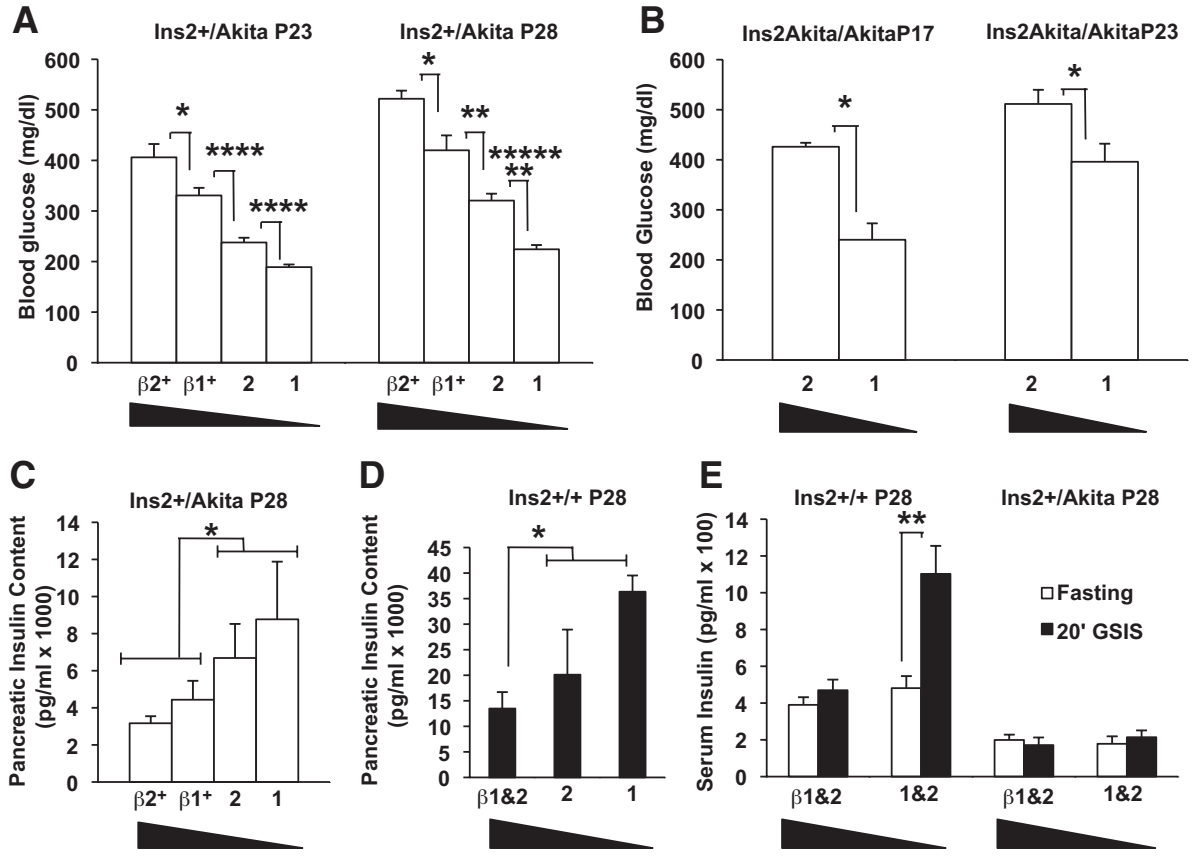

FIG. 7. *Perk* gene dosage modulates diabetic progression of the *Akita* mouse. *A–E*: Four Perk genotypes, including $Perk^{+/+}$ ("2"), $Perk^{+/-}$ ("1"), *βPerk;*$Perk^{+/+}$ ("β2"), and *βPerk;*$Perk^{+/-}$ ("β1"), were crossed to $Ins2^{+/Akita}$ mice to assess glucose homeostasis and insulin in the resulting strains. The expression of *Perk* mRNA is elevated ~80% above normal in *βPerk;*$Perk^{+/+}$ in β-cells. *A*: Progression toward overt diabetes in $Ins2^{+/Akita}$ mutant is positively correlated with increasing *Perk* gene dosage. Blood glucose was measured at P23 and P28 in the same group of mice (β2: $n = 11$, β1: $n = 11$, 2: $n = 45$, 1: $n = 42$; *$P < 0.05$, **$P < 0.005$, ****$P < 0.00005$, *******$P < 0.00000005$). *B*: Random blood glucose levels measured in P17 and P23 $Ins2^{Akita/Akita}$ mutant mice show that higher blood glucose levels are associated with an increase in *Perk* gene dosage (2: $n = 6$, 1: $n = 10$; *$P < 0.05$). *C*: Pancreatic insulin content decreases with increasing *Perk* gene dosage in the $Ins2^{+/Akita}$ mice. The insulin content of *Perk* wild-type and heterozygous mice with the *βPerk* transgene (β1 and β2) were pooled ($n = 12$) and compared with mice without the *βPerk* transgene (1 and 2) ($n = 12$) and found to be significantly different (*$P = 0.03$). *D*: Pancreatic insulin content decreases with increasing *Perk* gene dosage in the $Ins2^{+/+}$ mice (β1 and β2, $n = 10$; 1 and 2, $n = 8$). The difference between mice with and without *βPerk* transgene is statistically significant (*$P = 0.02$). *E*: An increase in *Perk* gene dosage was found to lead to an ablation of in vivo GSIS in P28 $Ins2^{+/+}$ mice (β1 and β2: $n = 12$, 1 and 2: $n = 11$; **$P < 0.005$). P28 $Ins2^{+/Akita}$ littermates demonstrated lower fasting serum insulin levels and impaired GSIS independent of *Perk* gene dosage (β1 and β2: $n = 11$, 1 and 2: $n = 10$).

proinsulin and insulin levels within the β-cells are dramatically reduced in both $Ins2^{+/Akita}$ heterozygotes and $Ins2^{Akita/Akita}$ homozygotes compared with robust expression of glucagon in neighboring α-cells (supplementary Fig. S5). We crossed the $Ins2^{+/Akita}$ heterozygotes with mice that were also heterozygous for *Perk* and found that the double heterozygous ($Ins2^{+/Akita}$; $Perk^{+/-}$) mice exhibited a substantial delay in developing diabetes compared with the $Ins2^{+/Akita}$; $Perk^{+/+}$ mice (Fig. 7*A*). Increasing *Perk* gene dosage, specifically in the β-cells of the *Akita* heterozygotes, by genetically introducing the wild-type *Perk* gene under the control of a truncated rat *Ins2* promoter (*βPerk*) (7), had the opposite effect by further accelerating the progression to overt diabetes (Fig. 7*A*). The more rapid progression to diabetes seen in the *Akita* homozygous mice was also delayed by reducing *Perk* dosage (Fig. 7*B*). Total pancreatic insulin content was inversely correlated with serum glucose as a function of *Perk* dosage in the $Ins2^{+/Akita}$ mice (Fig. 7*C* compared with Fig. 7*A*). Increasing *Perk* gene dosage in the β-cells of wild-type $Ins2^{+/+}$ mice (*βPerk*) also decreased pancreatic insulin content (Fig. 7*D*) and in vivo GSIS (Fig. 7*E*). In vivo GSIS and basal serum insulin was repressed in the $Ins2^{+/Akita}$ mice independent of *Perk* genotype (Fig. 7*E*). However, no significant increase was seen in apparent β-cell death in the *Akita* mice as assessed by TUNEL analysis (Table 1), nor was the proapoptotic *Chop* (GADD153) gene expression elevated. Even more surprisingly, β-cell mass and islet size was significantly expanded in $Ins2^{+/Akita}$ mice (Table 1) during the time that these mice are rapidly progressing to frank diabetes.

DISCUSSION

The diabetes seen in PERK-deficient humans and mice was speculated to be caused by dysfunctions in the ER stress response, including derepressed protein synthesis (8,9). However, we found that protein synthesis and proinsulin synthesis is not derepressed in *Perk*-deficient islets or other cell types that we have examined (12,13), and the majority of β-cells in *Perk KO* mice have no increase in proinsulin and have a significant reduction in insulin content. Therefore, the observed accumulation of proinsulin in the PERK-deficient β-cells, which exhibit the impacted-ER phenotype, is not caused by runaway protein synthesis. Rather, we found severe ablation of ER-Golgi

anterograde trafficking, disruption of the Golgi complex, reduced retrotranslocation of proteins out of the ER, and a decrease in proteasomal activity that together provide an explanation for the accumulation of proinsulin in the ER and insulin insufficiency.

Possible PERK-dependent factors that impact multiple ER functions are the chaperone/folding proteins GRP78/BiP, ERp72, and ERO1β. We found that BiP and ERp72 are substantially increased upon acute ablation of PERK in 832/13 β-cells (13) and exhibited enhanced expression in the impacted-ER β-cells in mouse islets, whereas ERO1β is reduced in islets (11,13). Modulating the expression of these ER chaperones can have a multiplicity of effects because these proteins are essential for folding, anterograde trafficking, and quality control (21,25,26). Increasing the expression of BiP may result in enhanced retention of client proteins in the ER by impeding anterograde trafficking and secretion (25). Elevated expression of ERp72 also increases ER retention and impedes the retrotranslocation step in ERAD (21). Genetic ablation of ERO1β has recently been shown to negatively impact glucose homeostasis (27). We speculate that PERK may regulate the competitive balance among ER chaperones that promotes either anterograde trafficking or ERAD of client proteins.

Two findings support the hypothesis that PERK primarily regulates ERAD. First, by tagging proinsulin with an ER retention signal we reduced the possibility of anterograde trafficking. Yet, we found that proinsulin still accumulated at much higher levels in the ER when *Perk* was impaired, suggesting that accumulation of proinsulin in *Perk KO* β-cells is caused by a failure in ERAD rather than anterograde trafficking. Second, the impact of altering *Perk* gene dosage in the *Akita* mouse suggests that *Perk* promotes ERAD. We found that decreasing *Perk* gene dosage by half ameliorates the progression of the *Akita* mouse to overt diabetes, whereas increasing *Perk* gene dosage in the β-cells of the *βPerk* transgenic mouse hastens progression to diabetes. Initially, it was proposed that increased β-cell death was the cause of the dominant Akita phenotype (28,29). However, we found substantially higher β-cell mass in *Akita* mice compared with wild-type at the onset of diabetes, and we failed to see an increase in TUNEL-positive β-cells. Although β-cell mass is not reduced at the onset of diabetes in *Akita* mice, insulin secretion is severely reduced (23). We speculate that the observed increase in β-cell mass is due to a compensatory response to reduced insulin secretion. Recent studies (30,31) have suggested that the Ins^{Akita} allele acts dominantly to enhance degradation of both the *Akita* and wild-type proinsulin via the ERAD pathway, and we propose that *Perk* acts to modulate the level of wild-type proinsulin degradation stimulated by the Ins^{Akita} mutation. Under this hypothesis, reducing *Perk* gene dosage decreases ERAD, thus sparing the degradation of wild-type proinsulin; whereas, increasing PERK dosage enhances the degradation of wild-type proinsulin, thus reducing secreted insulin even further.

Two ERAD processes were found to be impaired in *Perk*-deficient β-cells, retrotranslocation and proteasomal degradation, which raises the question if they are interconnected. Although the proteasome is localized in the cytoplasm, the 20S precursor is assembled at the ER membrane (22). ER dysfunctions or stress can impede proteasomal degradation of proteins (32), and mutations in proteins that regulate retrotranslocation can also impair general proteasomal activity (33). In addition to reduced general proteasomal activity, the 20S proteasome precursor was greatly diminished in the impacted-ER β-cells of *Perk KO* mice (Fig. 6*E*), suggesting that assembly or synthesis of the proteasome may be negatively impacted. Inhibition of proteasomal activity by MG132 also phenocopied the accumulation of proinsulin in the ER observed in *Perk*-deficient β-cells, consistent with the hypothesis that *Perk* may positively regulate ERAD.

Perk deficiency also results in dramatic changes in organelle structure and ER membrane composition in a substantial fraction of the β-cells. The Golgi apparatus, which normally displays a compact perinuclear localization, is dispersed and no longer distinct from the ER. The activation of the transcription factor ATF6 is also dependent upon the maintenance of ER and Golgi integrity, and we found that that the processed nuclear form of ATF6 was constitutively expressed in PERK-deficient β-cells, which is most likely due to mislocalization of the Golgi-processing enzymes S1P and S2P into the ER. This is consistent with the role of ATF6 as a negative regulator of insulin gene transcription (16,34) and reduced insulin mRNA levels in PERK-suppressed β-cells in culture (13) and in neonatal mice (11).

We have previously reported that *Perk*-deficient mice have a low β-cell mass due to decreased levels of β-cell proliferation during the critical late-embryonic to early neonatal stages of life (11). Moreover, β-cell proliferation is also reduced in insulinomas of Perk-deficient mice (35). How might the defects in ER functions and organelle integrity impact β-cell proliferation? First, normal proteasomal activity is necessary for cell-cycle progression (36), and we found that proteasomal activity was reduced. Second, the integrity of the ER and Golgi are normally maintained at all stages of mitosis (37). The disruption in the normal subcellular organization of these two organelles along with the defect in proteasomal activity (36) likely causes the reduced proliferation of β-cells in *Perk*-deficient mice.

We speculate that the major function of PERK in the β-cells is to act as a metabolic sensor that regulates proinsulin degradation in concert with metabolic demand for insulin. PERK enzymatic activity is negatively regulated by GRP78/BiP, when bound to calcium (38). Disassociation of GRP78/BiP-Ca^{2+} from PERK results in dimerization, autophosphorylation, and activation of its catalytic activity to phosphorylate eIF2α (38,39). PERK activity can be activated by dynamic changes in ER calcium that occur during fasting and glucose-stimulated insulin secretion without ever causing an apparent ER stress response (9,40). Following a brief fasting period, the activation of PERK is increased, whereas treatment of islets in culture with high glucose represses PERK's activity. We suggest that the function of PERK is to regulate proinsulin turnover in response to reduced nutrient intake when the demand for insulin is reduced.

ACKNOWLEDGMENTS

This work was supported by the National Institutes of Health Grants DK-062049 and GM-056957; the Pennsylvania Department of Health, Tobacco Settlement Funds (to D.R.C.); and a predoctoral fellowship from the American Heart Association (to S.G.).

No potential conflicts of interest relevant to this article were reported.

S.G., B.M., and D.C. wrote the manuscript and researched data.

We thank Kaori Iida, Rong Wang, Hanna Xu, Ajin Wang, Wenli Hu, and Siying Zhu for technical assistance. We thank Fumihiko Urano and Rajarshi Ghosh for the *shPerk* and *shScramble* 832/13 β-cell lines, Christopher Newgard for the INS1-832/13 cell line, Wayne I. Lencer (Harvard Medical School) for the CT-A antibody, J.J. Monaco (University of Cincinnati) for the C8 antibody, Jennifer Lippincott-Schwartz (National Institutes of Health) for the *ts045* VSVG-GFP construct, Peter Arvan and Ming Liu (University of Michigan) for the (human) wild-type proinsulin and the (human) C(B19)A mutant proinsulin constructs, Kazutoshi Mori (Kyoto University) for the pCMV*short*-EYFP-ATF6α construct, Ron Prywes (Columbia University) for the pCGN-HA-S2P construct, and David Ron (Skirball Institute) for the C terminus deleted 9E10 tagged mouse PERK (dominant negative) construct. We also acknowledge the assistance of the Melissa Rolls Lab (Penn State) with confocal microscopy and the Kouacou Konan Lab (Penn State) with subcellular fractionation experiments.

REFERENCES

1. Hou JC, Min L, Pessin JE. Insulin granule biogenesis, trafficking and exocytosis. Vitam Horm 2009;80:473–506
2. MacDonald PE, Joseph JW, Rorsman P. Glucose-sensing mechanisms in pancreatic beta-cells. Philos Trans R Soc Lond B Biol Sci 2005;360:2211–2225
3. Scheele GA. Regulation of pancreatic gene expression in response ot hormones and nutritional substrates. In *The Pancreas Biology, Pathobiology and Disease*. Go VLW, Ed. New York, Raven Press, 1993, p. 103–120
4. Arvan P. Secretory protein trafficking: genetic and biochemical analysis. Cell Biochem Biophys 2004;40:169–178
5. Orci L, Ravazzola M, Perrelet A. (Pro)insulin associates with Golgi membranes of pancreatic B cells. Proc Natl Acad Sci U S A 1984;81:6743–6746
6. Senee V, Vattem KM, Delepine M, Rainbow LA, Haton C, Lecoq A, Shaw NJ, Robert JJ, Rooman R, Diatloff-Zito C, Michaud JL, Bin-Abbas B, Taha D, Zabel B, Franceschini P, Topaloglu AK, Lathrop GM, Barrett TG, Nicolino M, Wek RC, Julier C. Wolcott-Rallison Syndrome: clinical, genetic, and functional study of EIF2AK3 mutations and suggestion of genetic heterogeneity. Diabetes 2004;53:1876–1883
7. Li Y, Iida K, O'Neil J, Zhang P, Li S, Frank A, Gabai A, Zambito F, Liang SH, Rosen CJ, Cavener DR. PERK eIF2alpha kinase regulates neonatal growth by controlling the expression of circulating insulin-like growth factor-I derived from the liver. Endocrinology 2003;144:3505–3513
8. Harding HP, Zeng H, Zhang Y, Jungries R, Chung P, Plesken H, Sabatini DD, Ron D. Diabetes mellitus and exocrine pancreatic dysfunction in perk-/- mice reveals a role for translational control in secretory cell survival. Mol Cell 2001;7:1153–1163
9. Zhang P, McGrath B, Li S, Frank A, Zambito F, Reinert J, Gannon M, Ma K, McNaughton K, Cavener DR. The PERK eukaryotic initiation factor 2 alpha kinase is required for the development of the skeletal system, postnatal growth, and the function and viability of the pancreas. Mol Cell Biol 2002;22:3864–3874
10. Wei J, Sheng X, Feng D, McGrath B, Cavener DR. PERK is essential for neonatal skeletal development to regulate osteoblast proliferation and differentiation. J Cell Physiol 2008;217:693–707
11. Zhang W, Feng D, Li Y, Iida K, McGrath B, Cavener DR. PERK EIF2AK3 control of pancreatic beta cell differentiation and proliferation is required for postnatal glucose homeostasis. Cell Metab 2006;4:491–497
12. Iida K, Li Y, McGrath BC, Frank A, Cavener DR. PERK eIF2 alpha kinase is required to regulate the viability of the exocrine pancreas in mice. BMC Cell Biol 2007;8:38
13. Feng D, Wei J, Gupta S, McGrath BC, Cavener DR. Acute ablation of PERK results in ER dysfunctions followed by reduced insulin secretion and cell proliferation. BMC Cell Biol 2009;10:61
14. Presley JF, Cole NB, Schroer TA, Hirschberg K, Zaal KJ, Lippincott-Schwartz J. ER-to-Golgi transport visualized in living cells. Nature 1997;389:81–85
15. Adachi Y, Yamamoto K, Okada T, Yoshida H, Harada A, Mori K. ATF6 is a transcription factor specializing in the regulation of quality control proteins in the endoplasmic reticulum. Cell Struct Funct 2008;33:75–89
16. Seo HY, Kim YD, Lee KM, Min AK, Kim MK, Kim HS, Won KC, Park JY, Lee KU, Choi HS, Park KG, Lee IK. Endoplasmic reticulum stress-induced activation of activating transcription factor 6 decreases insulin gene expression via up-regulation of orphan nuclear receptor small heterodimer partner. Endocrinology 2008;149:3832–3841
17. Kaufman RJ, Scheuner D, Schroder M, Shen X, Lee K, Liu CY, Arnold SM. The unfolded protein response in nutrient sensing and differentiation. Nat Rev Mol Cell Biol 2002;3:411–421
18. Shen J, Prywes R. Dependence of site-2 protease cleavage of ATF6 on prior site-1 protease digestion is determined by the size of the luminal domain of ATF6. J Biol Chem 2004;279:43046–43051
19. Schubert U, Anton LC, Gibbs J, Norbury CC, Yewdell JW, Bennink JR. Rapid degradation of a large fraction of newly synthesized proteins by proteasomes. Nature 2000;404:770–774
20. Meusser B, Hirsch C, Jarosch E, Sommer T. ERAD: the long road to destruction. Nat Cell Biol 2005;7:766–772
21. Forster ML, Sivick K, Park YN, Arvan P, Lencer WI, Tsai B. Protein disulfide isomerase-like proteins play opposing roles during retrotranslocation. J Cell Biol 2006;173:853–859
22. Fricke B, Heink S, Steffen J, Kloetzel PM, Kruger E. The proteasome maturation protein POMP facilitates major steps of 20S proteasome formation at the endoplasmic reticulum. EMBO Rep 2007;8:1170–1175
23. Izumi T, Yokota-Hashimoto H, Zhao S, Wang J, Halban PA, Takeuchi T. Dominant negative pathogenesis by mutant proinsulin in the Akita diabetic mouse. Diabetes 2003;52:409–416
24. Stoy J, Edghill EL, Flanagan SE, Ye H, Paz VP, Pluzhnikov A, Below JE, Hayes MG, Cox NJ, Lipkind GM, Lipton RB, Greeley SA, Patch AM, Ellard S, Steiner DF, Hattersley AT, Philipson LH, Bell GI. Insulin gene mutations as a cause of permanent neonatal diabetes. Proc Natl Acad Sci U S A 2007;104:15040–15044
25. Dhahbi JM, Cao SX, Tillman JB, Mote PL, Madore M, Walford RL, Spindler SR. Chaperone-mediated regulation of hepatic protein secretion by caloric restriction. Biochem Biophys Res Commun 2001;284:335–339
26. Nehls S, Snapp EL, Cole NB, Zaal KJ, Kenworthy AK, Roberts TH, Ellenberg J, Presley JF, Siggia E, Lippincott-Schwartz J. Dynamics and retention of misfolded proteins in native ER membranes. Nat Cell Biol 2000;2:288–295
27. Zito E, Chin KT, Blais J, Harding HP, Ron D: ERO1-{beta}, a pancreas-specific disulfide oxidase, promotes insulin biogenesis and glucose homeostasis. J Cell Biol 188:821–832
28. Oyadomari S, Koizumi A, Takeda K, Gotoh T, Akira S, Araki E, Mori M. Targeted disruption of the Chop gene delays endoplasmic reticulum stress-mediated diabetes. J Clin Invest 2002;109:525–532
29. Araki E, Oyadomari S, Mori M. Endoplasmic reticulum stress and diabetes mellitus. Intern Med 2003;42:7–14
30. Allen JR, Nguyen LX, Sargent KE, Lipson KL, Hackett A, Urano F. High ER stress in beta-cells stimulates intracellular degradation of misfolded insulin. Biochem Biophys Res Commun 2004;324:166–170
31. Liu M, Hodish I, Rhodes CJ, Arvan P. Proinsulin maturation, misfolding, and proteotoxicity. Proc Natl Acad Sci U S A 2007;104:15841–15846
32. Menendez-Benito V, Verhoef LG, Masucci MG, Dantuma NP. Endoplasmic reticulum stress compromises the ubiquitin-proteasome system. Hum Mol Genet 2005;14:2787–2799
33. Lipson C, Alalouf G, Bajorek M, Rabinovich E, Atir-Lande A, Glickman M, Bar-Nun S. A proteasomal ATPase contributes to dislocation of endoplasmic reticulum-associated degradation (ERAD) substrates. J Biol Chem 2008;283:7166–7175
34. Nozaki J, Kubota H, Yoshida H, Naitoh M, Goji J, Yoshinaga T, Mori K, Koizumi A, Nagata K. The endoplasmic reticulum stress response is stimulated through the continuous activation of transcription factors ATF6 and XBP1 in Ins2+/Akita pancreatic beta cells. Genes Cells 2004;9:261–270
35. Gupta S, McGrath B, Cavener DR. PERK regulates the proliferation and development of insulin-secreting beta-cell tumors in the endocrine pancreas of mice. PLoS ONE 2009;4:e8008
36. Zheng B, Georgakis GV, Li Y, Bharti A, McConkey D, Aggarwal BB, Younes A. Induction of cell cycle arrest and apoptosis by the proteasome inhibitor PS-341 in Hodgkin disease cell lines is independent of inhibitor of nuclear factor-kappaB mutations or activation of the CD30, CD40, and RANK receptors. Clin Cancer Res 2004;10:3207–3215
37. Axelsson MA, Warren G. Rapid, endoplasmic reticulum-independent diffusion of the mitotic Golgi haze. Mol Biol Cell 2004;15:1843–1852
38. Bertolotti A, Zhang Y, Hendershot LM, Harding HP, Ron D. Dynamic interaction of BiP and ER stress transducers in the unfolded-protein response. Nat Cell Biol 2000;2:326–332
39. Ma K, Vattem KM, Wek RC. Dimerization and release of molecular chaperone inhibition facilitate activation of eukaryotic initiation factor-2 kinase in response to endoplasmic reticulum stress. J Biol Chem 2002;277:18728–18735

40. Liang SH, Zhang W, McGrath BC, Zhang P, Cavener DR. PERK (eIF2alpha kinase) is required to activate the stress-activated MAPKs and induce the expression of immediate-early genes upon disruption of ER calcium homoeostasis. Biochem J 2006;393:201–209
41. Ward TH, Polishchuk RS, Caplan S, Hirschberg K, Lippincott-Schwartz J. Maintenance of Golgi structure and function depends on the integrity of ER export. J Cell Biol 2001;155:557–570
42. Liu M, Li Y, Cavener D, Arvan P. Proinsulin disulfide maturation and misfolding in the endoplasmic reticulum. J Biol Chem 2005;280:13209–13212
43. Nadanaka S, Yoshida H, Kano F, Murata M, Mori K. Activation of mammalian unfolded protein response is compatible with the quality control system operating in the endoplasmic reticulum. Mol Biol Cell 2004;15:2537–2548
44. Harding HP, Zhang Y, Ron D. Protein translation and folding are coupled by an endoplasmic-reticulum-resident kinase. Nature 1999;397:271–274
45. Shang J, Gao N, Kaufman RJ, Ron D, Harding HP, Lehrman MA. Translation attenuation by PERK balances ER glycoprotein synthesis with lipid-linked oligosaccharide flux. J Cell Biol 2007;176:605–616
46. Kitiphongspattana K, Mathews CE, Leiter EH, Gaskins HR. Proteasome inhibition alters glucose-stimulated (pro)insulin secretion and turnover in pancreatic {beta}-cells. J Biol Chem 2005;280:15727–15734
47. Ridsdale A, Denis M, Gougeon PY, Ngsee JK, Presley JF, Zha X. Cholesterol is required for efficient endoplasmic reticulum-to-Golgi transport of secretory membrane proteins. Mol Biol Cell 2006;17:1593–1605
48. Nandi D, Woodward E, Ginsburg DB, Monaco JJ. Intermediates in the formation of mouse 20S proteasomes: implications for the assembly of precursor beta subunits. Embo J 1997;16:5363–5375